IEEE Open Journal of Vehicular Technology

Received 6 August 2024; accepted 29 August 2024. Date of publication 9 September 2024;
date of current version 30 September 2024. The review of this article was coordinated by Editor Divya Garikapati.

Digital Object Identifier 10.1109/OJVT.2024.3456035

Sliding Mode Control for Robust Path Tracking of Automated Vehicles in Rural Environments

JOSE MATUTE [1], SERGIO DIAZ [2], AND ALI KARIMODDINI [1] (Senior Member, IEEE)

[1]Department of Electrical and Computer Engineering, North Carolina Agricultural and Technical State University, Greensboro, NC 27411 USA
[2]TECNALIA Research and Innovation, Basque Research and Technology Alliance (BRTA) Derio, 48160 Bizkaia, Spain

CORRESPONDING AUTHOR: ALI KARIMODDINI (e-mail: akarimod@ncat.edu).

This work was supported in part by the U.S. Department of Transportation (USDOT) University Transportation Program (UTC) under Grant 69A3552348304 and in part by the North Carolina Department of Transportation (NCDOT) under Grant RP2022-16 and Grant TCE2020-03. The work of Sergio Diaz was supported in part by the MEDUSA Network program and in part by MICIN through CDTI under the EU's MRR, under Grant CER-2023101.

ABSTRACT Achieving robust path tracking is essential for efficiently operating autonomous driving systems, particularly in unpredictable environments. This paper introduces a novel path-tracking control methodology utilizing a variable second-order Sliding Mode Control (SMC) approach. The proposed control strategy addresses the challenges posed by uncertainties and disturbances by reconfiguring and expanding the state-space matrix of a kinematic bicycle model guaranteeing Lyapunov stability and convergence of the system. A state prediction is integrated into the developed SMC to mitigate response time delays. Furthermore, the controller integrates adaptive mechanisms to adjust time-varying parameters within the control formulation based on longitudinal velocity, thereby enhancing path-tracking performance and reducing chattering phenomena. The effectiveness of the proposed approach is comprehensively evaluated through simulations and experiments encompassing challenging driving scenarios characterized by high-curvature paths, varying altitudes, and sensor disturbances, typical in rural driving environments. Results demonstrate that disturbances have varying impacts depending on the type of sensor affected. Real-world tests validate these findings, offering practical insights for automated vehicle path-tracking implementation.

INDEX TERMS Automated vehicles, path tracking, robustness, rural environments, sliding mode control, vehicle control.

I. INTRODUCTION

The path-tracking task is essential in Automated Driving Systems (ADS), as it translates high-level planning trajectories into real-time steering control actions to operate seamlessly in complex environments. Proper path-tracking enables a vehicle to follow predefined routes accurately while avoiding drift-off courses with precise control. However, as ADS rely on sensors to perceive their surroundings, these are prone to noises and disturbances, inherent in dynamic driving environments where an accurate and comfortable ride experience must be ensured. The Sliding Mode Control (SMC) is a robust control technique that has proven to mitigate the effects of noise in sensor readings, external disturbances, and vehicle model inaccuracies, by adjusting a sliding surface dynamically to ensure the system remains close to a desired trajectory [1]. However, concerns about practical implementation are essential to achieve an optimal path-tracking performance that ensures adaptability, chattering suppression, and robustness.

Defining the vehicle model in the SMC path-tracking design is an important task. Studies like in [2] have proposed a model-free adaptive strategy with control input saturation, resulting in particularly advantageous in low-speed driving applications like parallel parking systems. Simpler approaches are also introduced, by employing basic kinematic models in the absence of slip motion [3], and with constant linear and angular velocities as control inputs [4]. The relatively simple architecture of these approaches makes them suitable for moderate driving speed scenarios with low lateral acceleration values. Building upon this foundation, [5] presents an effective control system incorporating a dynamic bicycle model to achieve lateral control at high speeds. More refined systems can incorporate tire models as presented in [6], offering the

potential for precise lateral control at high speeds. Selecting a vehicle model for path tracking involves balancing fidelity and complexity. High-fidelity models can potentially offer superior control during high lateral acceleration maneuvers (e.g., sharp turns or emergencies), but their complexity makes them less suitable for slower maneuvers [7]. Low-to-medium-fidelity models are better suited for less critical scenarios, prioritizing ease of implementation and parameter tuning processes essential to reduce chattering.

Chattering is a phenomenon that occurs in SMC systems, characterized by rapid, high-frequency oscillations of the system trajectory around the desired state, known as the sliding surface. Significant negative consequences may include mechanical wear, energy inefficiency, reduced control accuracy, and excitation of unmodeled dynamics. In the context of path tracking, the discontinuous nature of first-order SMC methods is often smoothed [8], [9], [10], employing continuous functions, backstepping integration, or parameter optimization techniques, which have proven to reduce chattering in the control actions partially. In contrast, higher-order SMC methods have demonstrated superior effectiveness in mitigating the amplitude of oscillations [11], [12], [13], specifically for path-tracking applications demanding rapid responses from actuators [14]. Among the high-order SMC approaches, the Super-Twisting Algorithm (STA) has been widely recognized for its robustness to matched uncertainties and disturbances [15], [16], [17], [18], [19], often incorporating additional elements like constant boundary layer thickness, nested adaptive laws, or vehicle dynamic observers to enhance robustness. However, the variable nature of the driving task is commonly ignored in many of these studies, as verification is conducted under constant velocity scenarios.

Integrating variable gains into SMC methods enhances control design flexibility and performance in the presence of time-varying parameters [20], inherent to path-tracking applications. Consequently, several studies have combined SMC with other techniques to adapt the gains to current driving environments. Fuzzy Logic (FL) approaches, like those in [21] and [22], leverage FL systems to adjust control parameters or gain scheduling adaptively. These approaches often work in conjunction with Neural Networks (NN) to further approximate nonlinearities in system dynamics. NN studies, [23] and [24] utilize them to estimate unmatched disturbances, approximate uncertainties, or even directly learn the control law. Beyond FL and NN, optimization techniques are also explored. In [25], a fractional-order gradient descent algorithm is used to fine-tune the SMC design specifically for reduced chattering. Additionally, model predictive control is integrated with SMC in [26] to anticipate future system behavior and optimize the control input accordingly. While combining SMC with other control techniques offers potential benefits like improved performance and robustness, this introduces additional complexity to the overall control design making the system more challenging to design and verify, especially for real-time applications.

The effectiveness of path-tracking controllers is often evaluated involving various driving scenarios that challenge their ability to handle disturbances and uncertainties. Studies like [27], [28], [29] all explore the robustness of their proposed controllers through driving maneuvers like double lane changes and collision avoidance at varying road conditions. These scenarios introduce complexities like changing lateral dynamics, parametric uncertainties, and external disturbances like side wind. However, a notable limitation is the dominance of constant speed tests. While some studies, like [12], explore a wider range of speeds, time-varying velocity profiles are not frequently addressed. Notably, [30] goes beyond constant conditions and incorporates sensor noise in the yaw rate measurement, highlighting the importance of testing against real-world sensor limitations. Considering time-varying velocity references and sensor noises in tests, a more reliable assessment for realistic driving conditions can be provided.

This paper proposes a novel path-tracking approach based on SMC that prioritizes robustness against sensor noise in dynamic driving scenarios. It utilizes an improved kinematic vehicle model for effective adaptation to various operational conditions. The method suppresses chattering without complex gain adaptation, preserving the simplicity of a second-order SMC and streamlining implementation. Results show path-tracking accuracy and comfort comparable to state-of-the-art methods, even under unpredictable conditions. The practical implications are significant, offering a robust and easily implementable solution for automated vehicles, potentially improving safety and reliability in real-world situations. The main contributions of this work include:

- The development of a novel second-order SMC design by reconfiguring and expanding the state-space matrix of a kinematic bicycle model, ensuring Lyapunov stability converging towards the equilibrium point (zero tracking error). The developed kinematic bicycle model is also employed for state predictions, reducing the impact of time delays in path-tracking performance.
- The development of an adaptive mechanism to smooth the control actions and minimize the chattering phenomena. The developed mechanism can adjust the SMC parameters to the longitudinal velocity, ensuring effective control over the entire operation range.
- The developed controller is seamlessly integrated into Autoware, an open-source software stack for automated driving, which is made publicly available.[1]
- The verification through comprehensive simulations benchmarking the developed controller against state-of-the-art control mechanism and evaluating control stability under sensor disturbances in measurements.
- The validation of the proposed controller through real-world testing in a challenging test track, including speed variations, high-curvature paths, and altitude changes.

[1] https://github.com/ACCESSLab/smc-lateral-controller.git

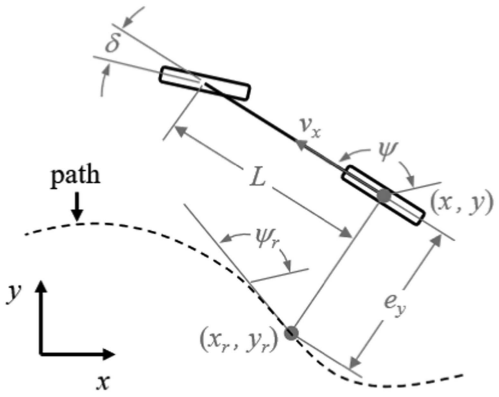

FIGURE 1. Kinematic bicycle model in path coordinates.

This paper is structured as follows: Section II delineates the employed vehicle model within the SMC system, encompassing both nonlinear and linear models, along with the formulations for state prediction. Section III elaborates on the design of the SMC control, elucidating aspects such as the sliding surface, boundary layer, and STA. Section IV delves into the methods for analytical and numerical analysis utilized to evaluate the stability of the proposed controller. Subsequently, Section V highlights pivotal aspects concerning integrating the developed SMC into Autoware, including details regarding the simulation environment and maps utilized for the testing route. Section VI outlines the testing scenarios and setup essential for discussing the results pertinent to benchmark comparison of the developed SMC with other controllers and its robustness to sensor disturbances. Finally, Section VII presents the conclusions drawn from the study.

II. VEHICLE MODEL

The kinematic bicycle model is employed in the control design, providing a simplified yet sufficiently accurate representation of the vehicle dynamics. This approximation involves collapsing the left and right wheels into a pair of single wheels at the center of the front and rear axles as depicted in Fig. 1.

This section dives into the kinematic bicycle model, explaining its linear and nonlinear forms related to the reference path. It also explores a formulation based on this model, which allows for predicting the future positions of the vehicle.

A. NONLINEAR VEHICLE MODEL

The nonlinear version of the kinematic bicycle model is articulated in terms of path coordinates and considers front-wheel steering only as in (1).

$$\dot{x} = \begin{bmatrix} \dot{e}_y \\ \ddot{e}_y \\ \dot{e}_\psi \\ \ddot{e}_\psi \end{bmatrix} = \begin{bmatrix} \sin(e_\psi) \\ \cos(e_\psi)\dot{e}_\psi \\ \tan(\delta)/L \\ 0 \end{bmatrix} v_x \tag{1}$$

where x is the current state of the vehicle, e_y is the lateral error (rear axle-to-path distance), e_ψ is the heading error (vehicle-to-path orientation difference), L is the wheelbase (front-to-rear axle distance), and δ is the front-wheel angle command.

In this work, the nonlinear formulation from [31] to include time derivatives for the lateral ($\dot{e}_y$) and orientation ($\dot{e}_\psi$) errors in (1). This enhancement improves dynamic representation during rapid trajectory changes, increases adaptability to varying conditions, and extends the operational range of kinematic bicycle models beyond low-speed scenarios [32]. Consequently, the model becomes more robust and suitable for diverse driving situations.

B. LINEARIZED VEHICLE MODEL

Linear kinematic models are ideal for SMC design due to their simplicity, efficiency, and compatibility with established methods [10], [25], [32]. The robustness to uncertainties allows SMC to work effectively even within the validity range of the kinematic bicycle model (e.g., low lateral accelerations).

The path tracking error model in (1) is linearized around the reference variables (i.e, v_x and δ_r) as illustrated in (2):

$$\dot{x} = \begin{bmatrix} 0 & 0 & v_x & 0 \\ 0 & 0 & 0 & v_x \\ 0 & 0 & 0 & 0 \\ 0 & 0 & 0 & 0 \end{bmatrix} x + \begin{bmatrix} 0 \\ 0 \\ \Gamma \\ 0 \end{bmatrix} \delta - \begin{bmatrix} 0 \\ 0 \\ \Gamma \\ 0 \end{bmatrix} \delta_r \tag{2}$$

where $x = [e_y, \dot{e}_y, e_\psi, \dot{e}_\psi]$ is the current state of the vehicle, the variable $\Gamma = v_x/(L \cdot \cos^2(\delta_r))$, the reference control input is $\delta_r = \arctan(L \cdot k_r)$, and k_r is the curvature of path.

In this work, both nonlinear and linear formulations are employed to thoroughly analyze global and local stability, respectively, ensuring robust performance across a wide range of operating conditions and around equilibrium points. Moreover, the linear formulation is employed for control design purposes due to its reasonable approximation within the operating range, making it suitable for the efficient implementation of SMC.

III. CONTROL DESIGN

This section focuses on the proposed control architecture design depicted in Fig. 2. The process starts by comparing the current position ($[x, y, \psi]$) with the reference trajectory ($[X_r, Y_r, \psi_r, k_r]$). This process yields the current tracking error state ($[e_y, \dot{e}_y, e_\psi, \dot{e}_\psi]$), which together with feedback gains (k_d), is used to forecast the future error state ($[e_{y,n}, \dot{e}_{y,n}, e_{\psi,n}, \dot{e}_{\psi,n}]$) needed for the proposed SMC. The specifics of this implementation are discussed in this section.

A. RECONFIGURING THE VEHICLE MODEL PREDICTIONS

The feedback values $k_d = -[K_y\ K_{\dot{y}}\ K_\psi\ K_{\dot{\psi}}]$ depend on the dynamics of the controlled plant and are used to reconfigure the diagonal elements of the state-space matrix in (2). Therefore,

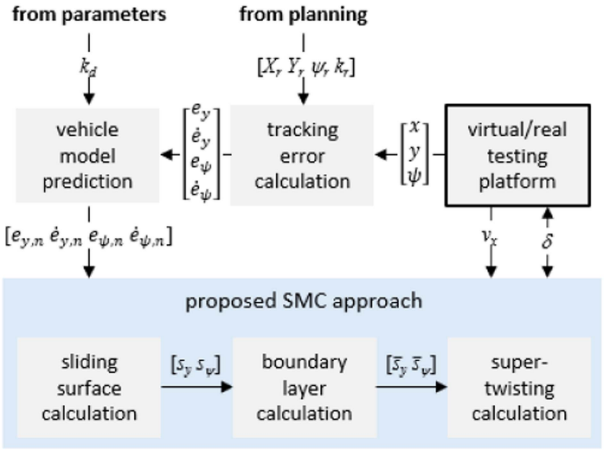

FIGURE 2. Control architecture design for the developed SMC.

Algorithm 1: Vehicle Model Prediction Algorithm.

procedure UpdatePredictionx_0, δ, v_x
  Get current errors $\leftarrow x_0 = [e_{y,0}, \dot{e}_{y,0}, e_{\psi,0}, \dot{e}_{\psi,0}]$
  for $i = 0, 1, \ldots, n$ **do** ▷ Iterate for n prediction steps
    Determine vehicle position $\leftarrow [X_i, Y_i, \psi_i]$
    Compute reference path curvature $\leftarrow k_{r,i}$
    Determine ideal steering angle $\leftarrow \delta_{r,i}$
    Compute kinematic factor $\Gamma_i \leftarrow v_x/(L \cdot \cos^2(\delta_{r,i}))$
    Predict next state using (3) $\leftarrow x_{i+1}$
  end for
  Store predicted state n $\leftarrow x_p = [e_{y,n}, \dot{e}_{y,n}, e_{\psi,n}, \dot{e}_{\psi,n}]$
  return x_p
end procedure

the linearized vehicle model is revisited next:

$$\dot{x} = \begin{bmatrix} -K_y & 0 & v_x & 0 \\ 0 & -K_y & 0 & v_x \\ 0 & 0 & -K_\psi & 0 \\ 0 & 0 & 0 & -K_\psi \end{bmatrix} x + \begin{bmatrix} 0 \\ 0 \\ \Gamma \\ 0 \end{bmatrix} \delta - \begin{bmatrix} 0 \\ 0 \\ \Gamma \\ 0 \end{bmatrix} \delta_r \tag{3}$$

This approach intends to reinforce the dissipation of energy or system motion, thereby promoting convergence towards zero tracking error. The effectiveness of this method will be confirmed through the stability analysis presented in Section IV.

The updating process of vehicle model predictions is outlined in Algorithm 1. Initially, the current vehicle coordinates ($[X, Y, \psi]$) are calculated based on the current states (x_0). Later, the curvature of the path (k_r), the reference control input (δ_r), and the variable Γ are computed to facilitate prediction estimation using (3). Ultimately, this algorithm returns a vector $x_p = [e_{y,n}, \dot{e}_{y,n}, e_{\psi,n}, \dot{e}_{\psi,n}]$.

Remark: The final differential system is given by the reconfigured kinematic model in (3), with the predicted states (x_p) acting as inputs to the sliding surface for computing control actions in the SMC implementation.

B. DESIGNING THE SLIDING SURFACE

The sliding surface consists of two functions defining the desired behavior of the system. To ensure that the lateral and orientation error trajectories converge and remain on the surfaces, the functions are designed as follows:

$$s_* = \dot{e}_{*,n_*} + \lambda \cdot e_{*,n_*} \tag{4}$$

where the sub-index $*$ represents either y or ψ, linking the formulation to lateral or orientation error parameters respectively. Specifically, s_* denotes the corresponding sliding surface, while λ is the sliding surface error gain.

C. DESIGNING THE VARIABLE BOUNDARY LAYER

An approach to mitigate chattering involves incorporating a boundary layer around the sliding surface, which replaces the discontinuous switching action with continuous control within this region [33]. While a constant thickness is commonly employed in boundary layer design, this approach may compromise control performance in dynamic and uncertain environments. This work aims to address this limitation by proposing a variable boundary layer thickness (ϕ), which adjusts based on the velocity of the vehicle, as detailed below:

$$\phi = \max(\check{\phi}, \phi \cdot v_x) \tag{5}$$

where $\check{\phi}$ is the minimum thickness value, and γ is the variable boundary layer gain. By dynamically adjusting ϕ with the value of v_x, the controller can adapt to a broad range of operating conditions, effectively balancing the trade-off between reducing chattering and maintaining robustness.

The smoothness of the continuous control action within the boundary layer region is enhanced as follows:

$$\bar{s}_* = \tanh(s_*/\phi) \tag{6}$$

where $\bar{s}_*$ represent smoothed approximation of s_*.

D. DESIGNING THE VARIABLE SUPER-TWISTING ALGORITHM

Second-order sliding mode control algorithms offer a robust solution to the chattering issue without sacrificing robustness properties. Among these, the super-twisting algorithm is a popular choice. By integrating a sliding mode control approach with a nonlinear sliding surface, it adjusts the control action according to the rate of change, ensuring smooth operation and robust performance as outlined below:

$$\delta_* = \delta_{1_*} + \delta_{2_*} \tag{7a}$$

$$\delta_{1_*} = -\alpha |\bar{s}_*|^{1/2} \bar{s}_* \tag{7b}$$

$$\dot{\delta}_{2_*} = -\beta \bar{s}_* v_x \tag{7c}$$

where α and β are the super-twisting gains for the error and its time derivative, respectively. Note in (7c) the addition of v_x in the rate of change of control action ($\dot{\delta}_{2_*}$), allowing the controller to adapt to the current operational condition.

The lateral and orientation errors are involved in the total control input estimation. The addition of both variables is traduced in an enhancement of the accuracy and stability of the controller, following the next formulation:

$$\delta = \Sigma\delta_* = \delta_y + \delta_\psi \tag{8}$$

where the sub-indexes y and ψ resulted from the substitution of the sub-index $*$ in (4)–(7), as stated in Section III-B.

IV. STABILITY ANALYSIS

This section describes the Lyapunov indirect and direct methods as critical aspects of the proposed control approach. Moreover, an analysis derived from numerical methods is comprehensively performed to verify the global asymptotical stability of the closed-loop system.

A. LYAPUNOV INDIRECT METHOD

This stability concept employs the reconfigured kinematic bicycle model from (3) to assess local stability around the equilibrium states (x^+). The feedback values $K_y = v_x$ and $K_\psi = 1$ are selected for simulations. Then, the eigenvalues (λ_s) of the state-space matrix are determined as follows:

$$\begin{vmatrix} \lambda_s + v_x & 0 & v_x & 0 \\ 0 & \lambda_s + v_x & 0 & v_x \\ 0 & 0 & \lambda_s + 1 & 0 \\ 0 & 0 & 0 & \lambda_s + 1 \end{vmatrix} = (\lambda_s + v_x)^2(\lambda_s + 1)^2 \tag{9}$$

As all the λ_s have strictly negative real parts ($-v_x$ and -1), the system in (3) is considered locally stable around x^+.

Remark: The eigenvalues estimated from the state-space matrix in the linearized form in (3) are evaluated to assess the local stability through the Lyapunov Indirect Method.

B. LYAPUNOV DIRECT METHOD

The application of this concept requires a nonlinear system to assess global stability. Adding the feedback k_d to (1), the reconfigured nonlinear vehicle model is described as follows:

$$\dot{x} = \begin{bmatrix} \dot{e}_y \\ \ddot{e}_y \\ \dot{e}_\psi \\ \ddot{e}_\psi \end{bmatrix} = \begin{bmatrix} -e_y + \sin(e_\psi) \\ -\dot{e}_y + \cos(e_\psi)\dot{e}_\psi \\ -e_\psi / v_x \\ -\dot{e}_\psi / v_x \end{bmatrix} v_x \tag{10}$$

The next candidate Lyapunov function is identified:

$$V(x) = V(e_y, \dot{e}_y, e_\psi, \dot{e}_\psi) = (e_y^2 + \dot{e}_y^2 + e_\psi^2 + \dot{e}_\psi^2)/2 \tag{11}$$

The candidate function is positive definitive because of $V(x) \geq 0$ for all non-zero states and $V(0) = 0$. Consequently, the time derivative of $V(x)$ along the system trajectories can be described as follows:

$$\dot{V}(t) = -(e_\psi^2 + \dot{e}_\psi^2) - (e_y^2 + \dot{e}_y^2)v_x + \zeta v_x \tag{12}$$

where $\zeta = e_y \sin e_\psi + \dot{e}_y \dot{e}_\psi \cos e_\psi$. To demonstrate that the time derivative of $V(x)$ is negative definitive, the next inequality must hold true:

$$(e_\psi^2 + \dot{e}_\psi^2) + (e_y^2 + \dot{e}_y^2)v_x > \zeta v_x \tag{13}$$

Observe that $(e_\psi^2 + \dot{e}_\psi^2) > 0$ and $(e_y^2 + \dot{e}_y^2)v_x > 0$ for all non-equilibrium states, however, ζv_x might be bigger in some specific cases as it is dependent of the state values signs. Assuming that the influence of ζv_x is minimal in the (12), the time derivative of $V(x)$ is potentially negative definitive.

Based on the previous analysis, the x^+ has the potential to be globally asymptotically stable because the function $V(x)$ seems to satisfy two main conditions: 1) $V(x)$ is positive definitive, and 2) $\dot{V}(t)$ is negative definitive. In this case, $V(x)$ can be considered a Lyapunov function.

However, since the assumption about the influence of ζv_x is insufficient to conclude the global asymptotic stability of x^+ definitively, additional numerical analysis is required to verify stability across a broader range of conditions and provide a more comprehensive understanding of the system behavior.

Remark: The nonlinear form in (10) is employed only for global asymptotical stability analysis, using the reconfigured form in (3) to implement the developed SMC method.

C. NUMERICAL ANALYSIS METHOD

Numerical stability analysis of the nonlinear system defined by (10) can provide valuable insights from visualizing the behavior of a system from initial state conditions over time.

The *quiver* function from the *matplotlib.pyplot*[2] library will create a 2D field of arrows (or vectors), which is useful for visualizing vector fields or flow data. In this case, the direction of each arrow denotes the direction of the state-space trajectory evolution at a particular point.

The *solve_ivp* function from the *scipy.integrate*[3] library will solve an initial value problem for the system of ordinary differential equations described in (10). A set of state-space trajectories will be generated for an initial set of conditions to cover all possible combinations of signs while checking the influence of ζv_x in the inequality described in (13).

D. STABILITY ANALYSIS

Fig. 3 depicts the vector fields and state-space trajectories of the dynamic system described by (10), considering specific initial conditions ($x_0 = [e_{y_0}, \dot{e}_{y_0}, e_{\psi_0}, \dot{e}_{\psi_0}]$). Each group of results (Figs. 3(a)–3(d)) contains 3D plots on the top, corresponding to the lateral error and its time-derivative phase plane, and 3D plots on the bottom, depicting their corresponding heading error and time-derivative phase plane. The cyan arrows (located on the 0s plane) represent the direction and magnitude of the vector field, which provide insights into the system behavior and how it evolves. The colored lines in red, green, orange, and blue, trace the system trajectories.

[2]https://matplotlib.org/3.5.3/api/_as_gen/matplotlib.pyplot.html
[3]https://docs.scipy.org/doc/scipy/reference/integrate.html

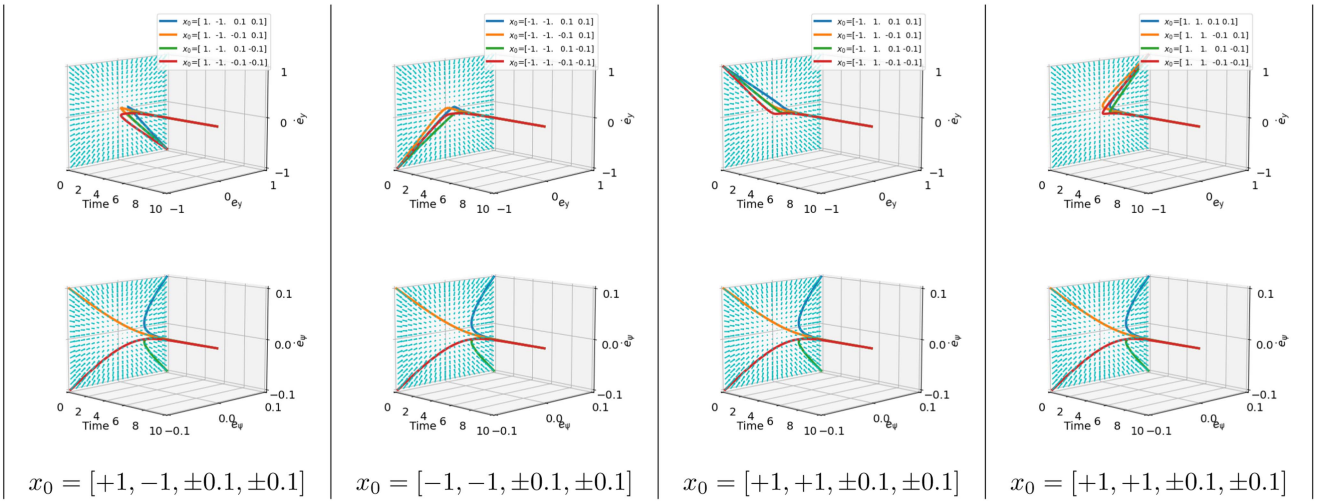

FIGURE 3. Vector field (cyan arrows) and state-space trajectories (blue, orange, green, and red lines) after 10 s of simulation time, showing lateral (top) and orientation (bottom) errors from different initial conditions ($x_0 = [e_{y_0}, \dot{e}_{y_0}, e_{\psi_0}, \dot{e}_{\psi_0}]$) and $v_x = 10$ m/s.

The stability analysis encompassed 16 simulations, systematically exploring all combinations in x_0 (i.e., all possible combinations of values for $[e_{y_0}, e_{\psi_0}, \dot{e}_{y_0}, \dot{e}_{\psi_0}]$, where each is defined as $[\pm 1, \pm 1, \pm 0.1, \pm 0.1]$, respectively). These simulations are divided into four groups (Figs. 3(a)–3(d)), depicted side by side, for easy visualization. A constant velocity of $v_x = 10$ m/s was deliberately chosen to induce unstable responses from the dynamical system.

The vector fields for both phase planes converge towards the stable equilibrium point ($x^+ = [0, 0, 0, 0]$), indicating system stability, with the lateral error plane (top row) and heading error plane (bottom row) describing a linear behavior as expected from the dynamical system after the negative feedback implementation. Thus, on the top row, bold patterns for the trajectories moving towards x^+ were obtained, elucidating the interplay between the lateral error (e_y) and its rate of change ($\dot{e}_y$). Notably, the trajectories and vector field exhibited an influence of v_x, e_ψ, and $\dot{e}_\psi$, inherent in the formulations of e_y and $\dot{e}_y$ in (10). Conversely, trajectories on the bottom row demonstrated softer patterns, delineating the relationship between the orientation error (e_ψ) and its rate of change ($\dot{e}_\psi$). Here, the shape of the trajectories is attributed to v_x being the sole influence on the behavior of e_ψ and $\dot{e}_\psi$ in (10).

The simulation outcomes provide evidence of the global asymptotic stability of the dynamical system analyzed in Section IV-B, indicating that under all pertinent initial conditions, the time derivative of the proposed Lyapunov function, as defined in (12), remains consistently negative. This signifies a continuous decrease in the energy over time, ultimately converging towards the x^+ characterized by zero lateral and orientation errors, before 5 s of simulation.

V. INTEGRATION TO AUTOWARE

The developed SMC is designed for seamless integration into Autoware built on ROS2 middleware. This section describes the planning simulator environment later employed for testing and evaluating the developed SMC, the rural testing route defined by point cloud and semantic maps, and the integration strategy of the SMC into the trajectory follower.

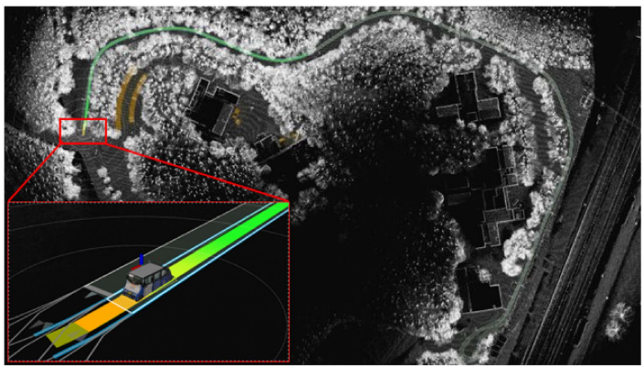

FIGURE 4. Visual of the planning simulator environment containing point cloud (white dots) and Lanelet2 (green areas) maps. The vehicle 3D model is in the starting position as shown on the lower left side. The goal location is set near the contiguous lane pointing in the opposite direction.

A. PLANNING SIMULATOR ENVIRONMENT

The planning simulator [34] is employed to verify the performance of the developed SMC. This simulator allows setting the point cloud and vector maps to customize the simulation according to the needs, where initial and goal poses can be settled for the ego vehicle to simulate specific scenarios. In this work, the vehicle and sensor models described in [35] are included in the simulator parameters. A visual from Rviz2 of the planning simulator is shown in Fig. 4.

B. MAPS FOR THE TESTING ROUTE

The testing route, a 1750-meter single-lane road on a closed test track at North Carolina A&T State University, was chosen for simulation to ensure consistency with future real vehicle

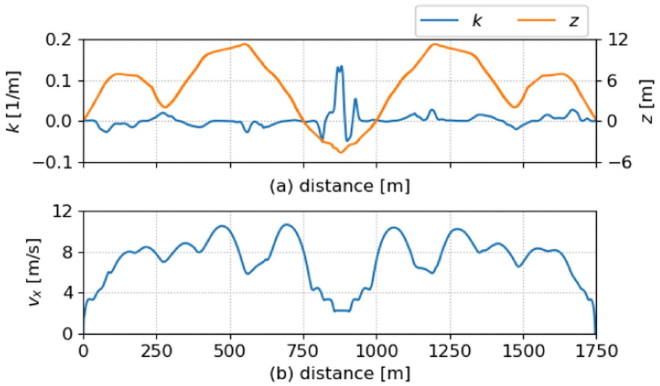

FIGURE 5. The (a) curvature (k) and altitude (z) characteristics of the route, and (b) longitudinal velocity (v_x) reference.

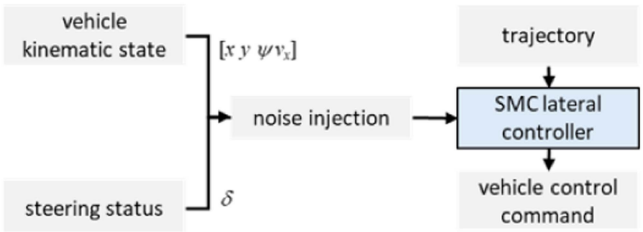

FIGURE 6. Leveraging Autoware for testing and evaluating the developed SMC method in a simulation environment.

testing. The creation process of the point cloud and Lanelet2 maps is described in [35]. Initially, Fig. 5(a) depicts the route curvatures (k) with values below 0.2 m^{-1} due to left and right turns. The altitude (z) varies by approximately 18m, indicating challenging terrain. Subsequently, Fig. 5(b) illustrates the speed reference utilized in simulations, adjusted to reduce speed reference during high-curvature segments, thereby improving path-tracking performance. The symmetry in k and z results from traversing half the route before returning near the starting point utilizing the single-lane road configuration.

C. SMC LATERAL CONTROLLER INTEGRATION

The SMC lateral controller is seamlessly integrated into the control module, utilizing pertinent variables obtained from the simulation testbed, such as the vehicle kinematic state ($[x, y, \psi, v_x]$) and steering status. Before their utilization in the control process, a failure injection procedure was devised to introduce disturbances into measurements for robustness assessment. Subsequently, the developed SMC leverages the potentially noisy variables alongside the reference trajectory to generate the Ackerman lateral command, delineated by the steering tire angle (δ). This process is depicted in Fig. 6.

During this study, the Autoware framework integrated the pure pursuit and model predictive control methods as the sole lateral controllers readily available. Hence, these existing controllers served as benchmarks to assess the performance of the developed SMC in simulations as discussed in Section VI-D.

VI. TESTING AND EVALUATING THE SMC

This section centers on the analysis results from testing and evaluating the developed SMC. It encompasses a comparative evaluation against benchmark controllers for path-tracking proficiency, and an assessment of robustness concerning disturbances affecting orientation, position, velocity, and steering angle measurements. The outcomes of the robustness assessment are normalized to illustrate the extent to which variations in sensor measurements affect path-tracking efficacy.

A. SIMULATION TESTING SCENARIOS

In evaluating the accuracy and reliability of the proposed controller, two verification approaches are conducted via simulation tests. Initially, the simulation environment depicted in Fig. 4 is utilized to compare the SMC approach with two other controllers established in the literature, in the measurement disturbances absence. Subsequently, employing the same route as in the previous test, varying levels of disturbances are introduced to the measurement of different sensors to evaluate the robustness of the controller, specifically in:

- *Position:* Signal interference from tall buildings, natural obstructions, or lack of positioning landmarks can cause errors leading to inaccuracies in position estimation [35].
- *Orientation:* Vibrations and shocks experienced by the vehicle, such as those from rough road surfaces or sudden acceleration/deceleration, can introduce noise and drift affecting orientation measurements.
- *Velocity:* Wheel slippage on slippery surfaces or irregularities in tire pressure can lead to inaccuracies in wheel speed measurements, affecting the velocity estimation.
- *Steering Angle:* Wear and tear in mechanical components or sensor misalignments can cause errors in angular measurements leading to inaccuracies in angle estimation.

In this study, the testing scenarios simulate the impact of random variations in sensor data, focusing on noise sensitivity without introducing bias for a more comprehensive evaluation of SMC performance under realistic noisy conditions. Particularly, Gaussian noises with three levels of standard deviation centered around the measured values, are examined in testing scenarios for; position (0.08, 0.16, and 0.32 m), orientation (0.02, 0.04, and 0.08 rd), velocity (0.32, 0.64, and 1.28 m/s), and steering angle (0.05, 0.01, and 0.02 rd) measurements.

The maximum tolerable noise levels were identified through trial and error, beyond which the proposed SMC method failed path-tracking, causing road departures or disabling motion planning in simulations. The employed noise levels are comparable to or less conservative than related literature [36].

B. EXPERIMENTAL TESTING PLATFORM

The testing platform consists of a Polaris GEM e6 as shown in Fig. 7, a six-passenger electric vehicle designed for short-range urban transportation with a maximum velocity of 40 km/h. The vehicle is equipped with a Velodyne VLP-32C

FIGURE 7. The automated shuttle employed for real tests.

TABLE 1. Parameter Values

Symbol	Parameter	Sim	Exp	Unit
λ	sliding surface error gain	24.0	10.0	-
α	super-twisting error gain	0.8		-
β	super-twisting derivative error gain	0.04	0.02	-
ϕ	variable boundary layer gain	1.0	0.5	-
$\check{\phi}$	lower boundary layer limit	1.0	2.0	-
n	prediction number	24	14	-
D	decay speed of steering command	0.9	0.2	m/s
$\hat{\Delta}\delta$	steering rate limit	-	0.3	rad/s
$\hat{\delta}$	steering angle limit	0.7		rad
f_s	lowpass filter cutoff (states)	1.0		Hz
f_c	lowpass filter cutoff (control)	3.0		Hz
Δs	path resampling interval	0.1		m

LiDAR sensor for high-precision localization, and a high-performance computing system comprising an Intel XEON E2278G CPU, NVIDIA RTX A4000 GPU, and a 1 TB NVMe M.2 2280 SSD. The SMC algorithm, as delineated in Section V, is implemented and deployed on a physical test track analogous to the simulated environment illustrated in Fig. 4. The system interfaces with the drive-by-wire mechanism of the automated shuttle via a CAN protocol, translating the output from the SMC algorithm, primarily the front wheel steering angle, into appropriate low-level control signals for steering actuation.

C. TESTING SETUP

The parameter values utilized in evaluating and implementing the proposed control architecture are shown in Table 1. These values were carefully chosen based on performance considerations to achieve robust and accurate control under diverse operating conditions including sensor disturbances.

It is important to note that the values chosen for simulations differ from those used in real-world testing. This discrepancy stems from the difference between the virtual and real platform dynamics, with the latter being more complex. Hence, the feedback gains defined in Section III-A were adapted to the real platform as $K_y = \max(2, v_x/2)$ and $K_\psi = 2$.

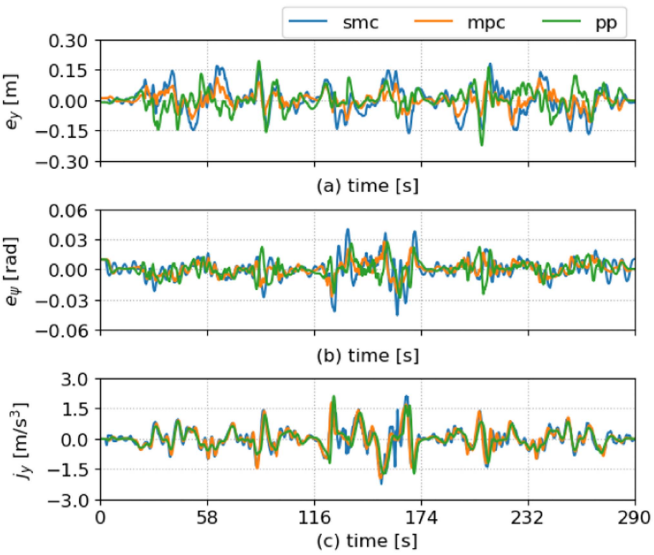

FIGURE 8. Comparison of (a) lateral error (e_y), (b) orientation error (e_ψ), and (c) lateral jerk (j_y) with benchmark controllers.

TABLE 2. Simulation Testings and Benchmark Controllers

metric	method	med	IQR	WR	max
e_y [m]	MPC	0.001	0.019	0.075	0.125
	PP	0.001	0.026	0.103	0.224
	SMC	0.001	0.040	0.160	0.181
e_ψ [rad]	MPC	0.000	0.004	0.016	0.028
	PP	0.001	0.001	0.014	0.028
	SMC	0.001	0.014	0.022	0.045
j_y [m/s^3]	MPC	0.000	0.237	0.948	1.947
	PP	0.005	0.235	0.936	2.124
	SMC	0.018	0.298	1.191	2.243

D. COMPARISON WITH BENCHMARK CONTROLLERS

Fig. 8 shows the outcomes derived from simulation tests aimed at assessing the efficacy of the Sliding Mode Control (SMC, in blue) technique introduced in this study, juxtaposed against two established path-tracking methodologies: Pure Pursuit (PP, in green) and Model Predictive Control (MPC, in orange). These evaluations were conducted under sensor disturbance-free conditions, as elucidated in Section VI-A. Figs. 8(a)–8(b) delineate the lateral and orientation errors, respectively, revealing that the SMC strategy achieves a precision comparable to that of both PP and MPC methods. Furthermore, Fig. 8(c) illustrates the lateral jerk response, providing evidence that the SMC method affords a similar level of comfort during the execution of path-tracking tasks compared to PP and MPC.

Table 2 furnishes a quantitative analysis delineating the performance of the three distinct controllers scrutinized in Fig. 8, encompassing metrics such as the median (med), interquartile range (IQR), whisker range (WR), and maximum (max) values for the lateral error (e_y), orientation error (e_ψ), and lateral jerk (j_y). In certain scenarios, the efficacy of the SMC methodology demonstrates enhancement relative to the Pure

TABLE 3. Median (med), Interquartile Range (IQR), Whisker Range (WR), and Maximum (max) Values for Lateral Error (e_y), and Orientation Error (e_ψ), and Lateral Jerk (j_y) Under Simulated Disturbance Levels in Sensors (σ_*) and Real Test Experiment

			σ_{xy} [m]			σ_ψ [rad]			σ_{vx} [m/s]			σ_δ [rad]			
	level	ref	0.08	0.16	0.32	0.02	0.04	0.08	0.32	0.64	1.28	0.05	0.01	0.02	exp
e_y	med	0.001	-0.002	0.000	0.001	0.006	0.008	0.017	-0.005	0.003	-0.001	0.000	-0.005	0.001	-0.036
	IQR	0.040	0.040	0.050	0.060	0.045	0.050	0.089	0.039	0.041	0.038	0.042	0.043	0.055	0.095
	WR	0.160	0.164	0.198	0.240	0.178	0.198	0.354	0.156	0.162	0.153	0.169	0.173	0.221	0.376
	max	0.181	0.219	0.2127	0.309	0.194	0.361	0.637	0.174	0.203	0.218	0.191	0.224	0.412	0.587
e_ψ	med	0.001	0.001	0.000	0.000	0.001	0.001	-0.000	0.001	0.000	0.000	0.001	0.001	0.001	0.000
	IQR	0.005	0.006	0.006	0.008	0.007	0.009	0.014	0.006	0.006	0.006	0.005	0.006	0.008	0.016
	WR	0.022	0.024	0.024	0.030	0.026	0.0372	0.055	0.026	0.023	0.025	0.022	0.024	0.032	0.065
	max	0.045	0.053	0.051	0.082	0.053	0.0597	0.095	0.0441	0.047	0.074	0.050	0.047	0.051	0.168
j_y	med	-0.018	-0.016	-0.017	0.000	-0.005	0.020	0.014	-0.011	-0.017	-0.035	-0.003	0.000	-0.011	0.000
	IQR	0.298	0.318	0.363	0.433	0.323	0.403	0.651	0.288	0.311	0.376	0.288	0.313	0.382	0.065
	WR	1.190	1.272	1.452	1.731	1.290	1.611	2.592	1.152	1.243	1.505	1.152	1.252	1.527	2.401
	max	2.243	2.906	4.409	4.615	2.573	2.8258	7.146	2.453	2.568	3.618	2.390	2.349	3.389	5.602

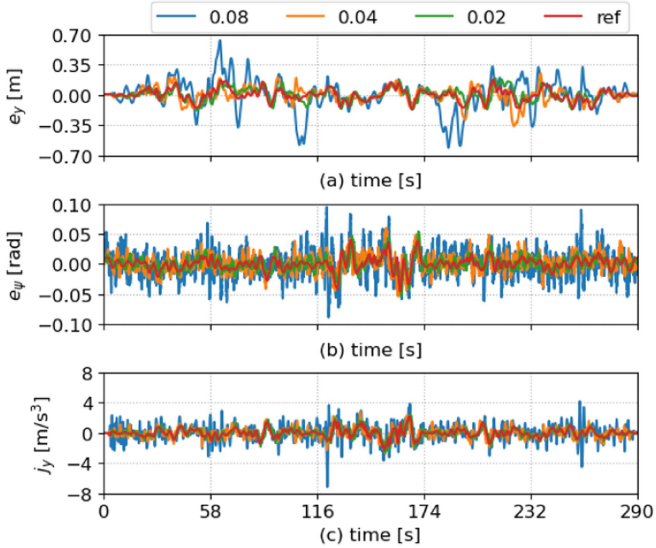

FIGURE 9. (a) Lateral error (e_y), (b) orientation error (e_ψ), and (c) lateral jerk (j_y) under disturbances in yaw measurements (σ_ψ = 0.02, 0.04, and 0.08 rad).

Pursuit (PP) approach, while overall, it exhibits a comparable performance to established path-tracking methodologies.

In this context, the IQR measures the spread of the middle 50% of the dataset, calculated as the difference between the upper and lower quartiles. The WR indicates the variability beyond the quartiles enclosing data within 1.5 times the IQR.

E. ROBUSTNESS TO SENSOR DISTURBANCES

Following the verification of safety and comfort capabilities through a driving scenario involving varied velocities and curvatures, free from measurement disturbances, the robustness of the developed SMC method is assessed in the same driving scenario by introducing varying levels of disturbances on those sensor measurements that directly impact the performance.

1) ORIENTATION DISTURBANCES

Fig. 9 illustrates the impact of varying levels of disturbances on the yaw measurement (σ_ψ) on tracking errors and lateral jerk response. As the disturbance value increases, indicated by the addition of Gaussian noise to the sensor measurement, there is a rapid degradation in path-tracking performance. Specifically, it becomes challenging to maintain lateral and orientation errors below 20cm and 0.03 rd, respectively, after a standard deviation of 0.04 rd of noise. However, the developed SMC method exhibits resilience, handling yaw disturbances up to 0.08 rd.

Yaw measurements are among the most sensitive sensors to disturbances, significantly influencing tracking performance.

2) POSITION DISTURBANCES

Table 3 presents the statistical outcomes derived from simulation tests conducted under varying levels of disturbances in sensor measurements. The initial column categorizes the tracking error and lateral jerk outcomes corresponding to different degrees of disturbances affecting position measurements (σ_{xy}). Notably, the developed SMC methodology demonstrates resilience in managing disturbances in position measurements with a standard deviation of up to 0.32 m, resulting in minor impacts on lateral error tracking. Conversely, an escalation in noise values exerts a more pronounced effect on orientation errors and lateral jerk.

Position emerges as comparatively less sensitive sensors to external disturbances, exerting a diminished influence on safety and comfort compared to yaw measurements. These findings are illustrated in Fig. 10(b) for ease of interpretation.

3) VELOCITY DISTURBANCES

The third column of Table 3 aggregates the tracking errors and lateral jerk outcomes associated with different levels of disturbances affecting longitudinal velocity measures (σ_{v_x}). Analogous to disturbances impacting position measures, disturbances in longitudinal velocity exhibit a minor effect on lateral tracking. However, in contrast to disturbances in position and yaw (Figs. 10(a)–10(b)) measurements, which result in an exponential deterioration of orientation tracking and lateral jerk, the escalation of noisy values in longitudinal velocity follows a linear trend. Specifically, the developed SMC approach demonstrates the ability to manage disturbances with a standard deviation of up to 1.28 m/s.

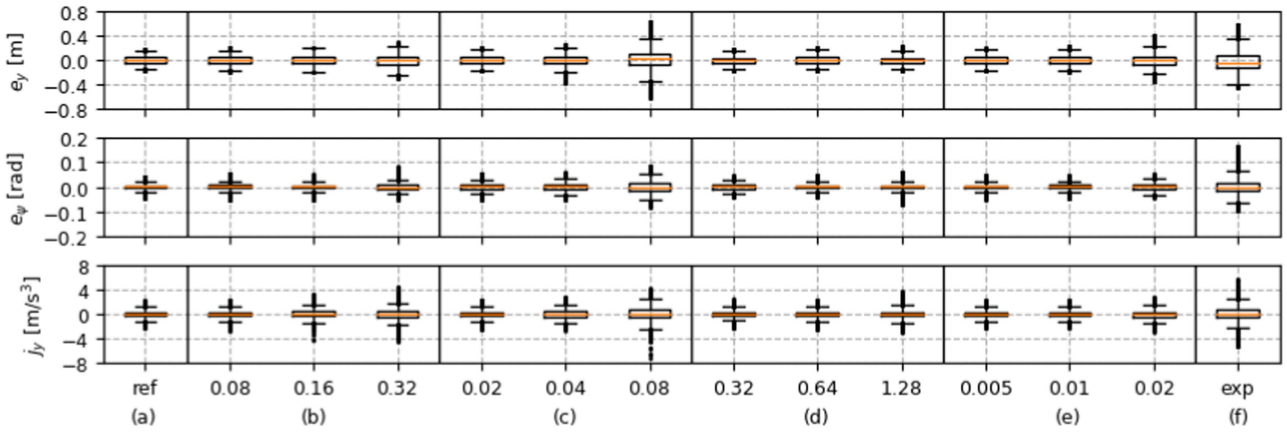

FIGURE 10. The statistical results of the sliding mode control are presented under various conditions, including the reference scenario with (a) no disturbances ($\sigma \approx 0$). The disturbances caused by Gaussian noises in sensors are characterized by standard deviations of (b) 0.08, 0.16, and 0.32 m around X and Y location coordinates ($\sigma_{x,y}$), (c) 0.02, 0.04, and 0.08 rad around the orientation angle (σ_ψ), (d) 0.32, 0.64, and 1.28 m/s around the longitudinal velocity (σ_{v_x}), and (e) 0.005, 0.01, and 0.02 rad around the front wheel steering angle (σ_δ). Experimental results are shown in (f).

Noise in longitudinal speed engenders the least impact on path-tracking performance. These observations are elucidated in Fig. 10(d) for enhanced comprehension.

4) STEERING ANGLE DISTURBANCES

The final column of Table 3 collates the tracking errors and lateral jerk outcomes corresponding to varying levels of disturbances on the steering angle measurements (σ_δ). Unlike disturbances affecting position and longitudinal velocity measurements, disturbances in the steering angle exhibit an exponential rather than linear effect on lateral tracking. Furthermore, concerning orientation tracking and lateral jerk, the impact remains minimal across the range of disturbances tested. The developed SMC method effectively managed disturbances up to a value of 0.02 rd.

Disturbances in steering angle measurements emerge as the most influential on safety, leading to a rapid deterioration in path-tracking performance. This observation is visually depicted in Fig. 10(e) to enhance comprehension.

5) NORMALIZED DISTURBANCES

Fig. 11 presents the results of a regression analysis applied to the whisker range (WR) values extracted from Table 3. The WR thoroughly understands the spread of responses due to sensor disturbances, capturing the variability beyond the upper and lower quartiles.

The WR values ($\hat{\sigma}_{xy}$, $\hat{\sigma}_\psi$, $\hat{\sigma}_{v_x}$, and $\hat{\sigma}_\delta$) were normalized by dividing them by a unit of the respective variable, thereby yielding a normalized disturbance variable (σ_*) for comparative analysis of different sensor disturbances in terms of lateral error (e_y), orientation error (e_ψ), and lateral jerk (j_y). The graphical depiction highlights the influence of varying magnitudes of sensor disturbances on safety and comfort.

As elucidated previously from Sections VI-E1 to VI-E4, disturbances affecting the steering angle (δ) and yaw (ψ) measurements exert the most significant impact on the dynamic driving task. In contrast, disturbances in position (xy) and longitudinal speed (v_x) elicit comparatively lesser effects on path-tracking performance.

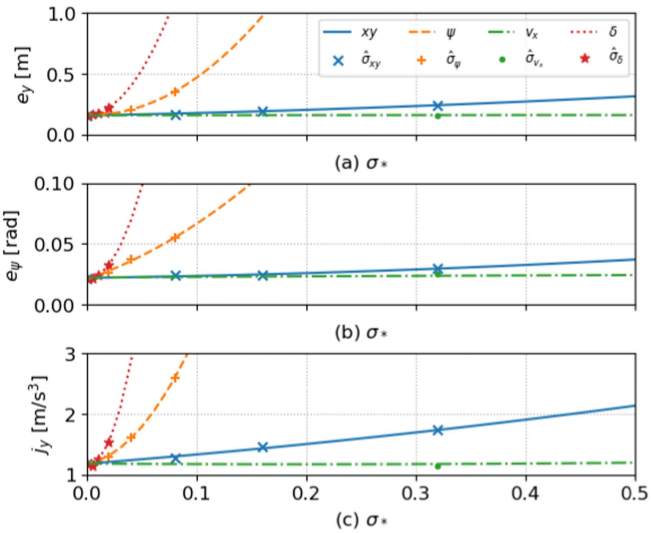

FIGURE 11. Linear regression of WR values for (a) lateral error (e_y), (b) orientation error (e_ψ), and (c) lateral jerk (j_x) with respect to sensor disturbances (σ_*).

F. REAL TEST EXPERIMENT

Fig. 12 demonstrates the SMC's performance in virtual and real-world tests. Real-world results aligned with simulations, maintaining IQR for e_y and e_ψ below 10 cm and 0.02 rd respectively (Table 3), indicating high path-tracking accuracy. Lateral jerk decreased in real tests due to simplified dynamics in the virtual platform. Peak errors occurred in the roundabout area (Fig. 12 zoom), with maximum e_y of 0.587 cm and e_ψ of 0.168 rd, attributed to real-world steering rate limits absent in

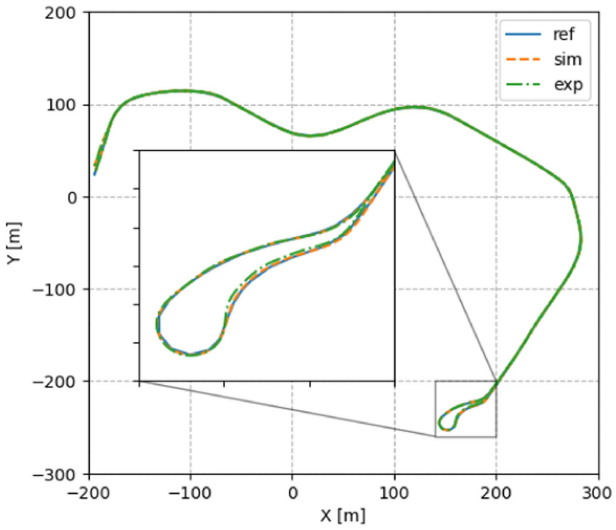

FIGURE 12. Comparative of simulation (sim) and experimental (exp) testing results on the path tracking performance concerning the planned path (ref) in XY coordinates. The zoom square highlights the tracking behavior at the roundabout zone.

simulations. The effectiveness of the developed Sliding Mode Control (SMC) is demonstrated in the accompanying video.[4]

Tuning the developed SMC starts with low values for the parameters λ and α. These values are then progressively increased to achieve optimal performance. Other parameters like β reduce the steady-state error of the tracking performance, ϕ significantly reduces chattering phenomena, and $\check{\phi}$ improves the performance at lower speeds while compromising the tracking accuracy. The value of n must align with the actuation delay, as wrong values deteriorate the tracking accuracy.

G. LIMITATIONS OF THE DEVELOPED SMC METHOD

While the developed SMC approach and the underlying extended kinematic bicycle model have demonstrated promising results, it is essential to acknowledge its limitations:

- *Curvature rates:* The developed SMC exhibits heightened sensitivity to abrupt curvature variations, particularly under sensor disturbances or during sharp turning maneuvers affecting the variability of curvature prediction.
- *Tolerable noises:* Beyond noise levels tested, both Autoware and the SMC method fail to perform path-tracking.
- *Slip conditions:* The proposed model assumes pure rolling conditions, which may not hold in low-friction surfaces.

VII. CONCLUSION

This paper presented a novel path-tracking control method for ADS using a variable second-order SMC approach. The developed SMC demonstrated its capability to handle various uncertainties and disturbances, typically encountered in real-world driving environments. The effectiveness of the SMC derived from its design elements, including negative feedback for convergence, prediction to overcome response delays, and combined chattering reduction methods. The adaptability of the proposed approach to time-varying parameters through velocity-dependent adjustments enhances its robustness.

The simulation and real-world outcomes demonstrate that the developed SMC method achieves precision and ride comfort levels during path-tracking, comparable to established methods like pure pursuit and model predictive control methods. Also, the robustness results highlight the stability and effectiveness of the SMC technique in challenging scenarios involving intricate paths, varying altitudes, and sensor noise, characteristic of rural driving environments. Finally, the linear regression analysis indicates that disturbances on the steering angle have the most impact on driving performance.

Future work will address current limitations by incorporating higher-fidelity models for robust state predictions, comparing the current approach with variable look-ahead distance systems, and exploring advanced control techniques for complex dynamics. Also, more benchmark controllers will be integrated into real-world tests for comprehensive comparative analysis.

[4][Online]. Available: https://youtu.be/aAkOmhhb00s

REFERENCES

[1] S. Ding and W. X. Zheng, "Nonsingular terminal sliding mode control of nonlinear second-order systems with input saturation," *Int. J. Robust Nonlinear Control*, vol. 26, no. 9, pp. 1857–1872, 2016.
[2] D. Xu, Y. Shi, and Z. Ji, "Model-free adaptive discrete-time integral sliding-mode-constrained-control for autonomous 4 WMV parking systems," *IEEE Trans. Ind. Electron.*, vol. 65, no. 1, pp. 834–843, Jan. 2018.
[3] M. O. Ortiz-García, R. Q. Fuentes-Aguilar, A. Palma-Zubia, and O. Carbajal-Espinosa, "Embedded control architecture for reference tracking of an automobile with actuated steering and brake systems," in *2022 IEEE Int. Symp. Electromobility*, 2022, pp. 1–6.
[4] J. Yang, R. Ma, Y. Zhang, and C. Zhao, "Sliding mode control for trajectory tracking of intelligent vehicle," *Phys. Procedia*, vol. 33, pp. 1160–1167, 2012.
[5] G. Tagne, R. Talj, and A. Charara, "Higher-order sliding mode control for lateral dynamics of autonomous vehicles, with experimental validation," in *2013 IEEE Intell. Veh. Symp.*, 2013, pp. 678–683.
[6] R. Khan, F. M. Malik, N. Mazhar, A. Raza, R. A. Azim, and H. Ullah, "Robust control framework for lateral dynamics of autonomous vehicle using barrier Lyapunov function," *IEEE Access*, vol. 9, pp. 50513–50522, 2021.
[7] J. A. Matute-Peaspan, M. Marcano, S. Diaz, A. Zubizarreta, and J. Perez, "Lateral-acceleration-based vehicle-models-blending for automated driving controllers," in *Electronics, vol.* 9, no. 10, 2020, Art. no. 1674.
[8] T. N. Kigezi, S. Alexandru, E. Mugabi, and P. I. Musasizi, "Sliding mode control for tracking of nonholonomic wheeled mobile robots," in *2015 IEEE 5th Australian Control Conf.*, 2015, pp. 21–26.
[9] A. Norouzi, M. Masoumi, A. Barari, and S. F. Sani, "Lateral control of an autonomous vehicle using integrated backstepping and sliding mode controller," *Proc. Inst. Mech. Engineers Part K: J. Multi-Body Dyn.*, vol. 233, no. 1, pp. 141–151, 2019.
[10] P. Wang, S. Gao, L. Li, S. Cheng, and L. Zhao, "Automatic steering control strategy for unmanned vehicles based on robust backstepping sliding mode control theory," *IEEE Access*, vol. 7, pp. 64984–64992, 2019.

[11] J. Liu, L. Gao, J. Zhang, and F. Yan, "Super-twisting algorithm second-order sliding mode control for collision avoidance system based on active front steering and direct yaw moment control," *Proc. Inst. Mech. Engineers, Part D: J. Automobile Engi.*, vol. 235, no. 1, pp. 43–54, 2021.

[12] D. Ao, W. Huang, P. K. Wong, and J. Li, "Robust backstepping super-twisting sliding mode control for autonomous vehicle path following," *IEEE Access*, vol. 9, pp. 123165–123177, 2021.

[13] H. Kim and S.-C. Kee, "Neural network approach super-twisting sliding mode control for path-tracking of autonomous vehicles," in *Electronics*, vol. 12, no. 17, 2023, Art. no. 3635.

[14] U. Pérez-Ventura and L. Fridman, "Chattering comparison between continuous and discontinuous sliding-mode controllers," in *Variable- Struct. Syst. Sliding-Mode Control: Theory Pract.*, vol. 271, pp. 197–211, 2020.

[15] Y. B. Shtessel, I. A. Shkolnikov, and M. D. Brown, "An asymptotic second-order smooth sliding mode control," *Asian J. Control*, vol. 5, no. 4, pp. 498–504, 2003.

[16] H. Imine and T. Madani, "Sliding-mode control for automated lane guidance of heavy vehicle," *Int. J. Robust Nonlinear Control*, vol. 23, no. 1, pp. 67–76, 2013.

[17] R. Solea and D. Cernega, "Super twisting sliding mode controller applied to a nonholonomic mobile robot," in *2015 IEEE 19th Int. Conf. System Theory Control Comput.*, 2015, pp. 87–92.

[18] Z. Sun, J. Zheng, Z. Man, M. Fu, and R. Lu, "Nested adaptive super-twisting sliding mode control design for a vehicle steer-by-wire system," *Mech. Syst. Signal Process.*, vol. 122, pp. 658–672, 2019.

[19] J. Chen, Z. Shuai, H. Zhang, and W. Zhao, "Path following control of autonomous four-wheel-independent-drive electric vehicles via second-order sliding mode and nonlinear disturbance observer techniques," *IEEE Trans. Ind. Electron.*, vol. 68, no. 3, pp. 2460–2469, Mar. 2021.

[20] G. P. Incremona, M. Rubagotti, M. Tanelli, and A. Ferrara, "A general framework for switched and variable gain higher order sliding mode control," *IEEE Trans. Autom. Control*, vol. 66, no. 4, pp. 1718–1724, Apr. 2021.

[21] H. Taghavifar and S. Rakheja, "Path-tracking of autonomous vehicles using a novel adaptive robust exponential-like-sliding-mode fuzzy type-2 neural network controller," *Mech. Syst. Signal Process.*, vol. 130, pp. 41–55, 2019.

[22] R. M. Shet, G. V. Lakhekar, and N. C. Iyer, "Design of quasi fuzzy sliding mode based maneuvering of autonomous vehicle," *Int. J. Dyn. Control*, vol. 12, pp. 1963–1986, 2024.

[23] K. Akermi, S. Chouraqui, and B. Boudaa, "Novel SMC control design for path following of autonomous vehicles with uncertainties and mismatched disturbances," *Int. J. Dyn. Control*, vol. 8, no. 1, pp. 254–268, 2020.

[24] B. Xing, E. Xu, J. Wei, and Y. Meng, "Recurrent neural network non-singular terminal sliding mode control for path following of autonomous ground vehicles with parametric uncertainties," *IET Intell. Transport Syst.*, vol. 16, no. 5, pp. 616–629, 2022.

[25] P. Li, T. Yang, H. Zhang, L. Wang, and Q. Li, "Lateral control of intelligent vehicles using radial basis function neural networks with sliding mode control based on fractional order calculus," *J. Intell. Manuf. Special Equip.*, vol. 3, no. 2, pp. 117–133, 2022.

[26] Y. Wu, L. Wang, F. Li, and J. Zhang, "Robust sliding mode prediction path tracking control for intelligent vehicle," *Proc. Inst. Mech. Engineers, Part I: J. Syst. Control Eng.*, vol. 236, no. 9, pp. 1607–1617, 2022.

[27] A. Barari, S. S. Afshari, and X. Liang, "Coordinated control for path-following of an autonomous four in-wheel motor drive electric vehicle," *Proc. Inst. Mech. Engineers Part C: J. Mech. Eng. Sci.*, vol. 236, no. 11, pp. 6335–6346, 2022.

[28] L. El Hajjami, E. M. Mellouli, and M. Berrada, "Robust adaptive non-singular fast terminal sliding-mode lateral control for an uncertain ego vehicle at the lane-change maneuver subjected to abrupt change," *Int. J. Dyn. Control*, vol. 9, pp. 1–18, 2021.

[29] B. Wang, Y. Lei, Y. Fu, and X. Geng, "Autonomous vehicle trajectory tracking lateral control based on the terminal sliding mode control with radial basis function neural network and fuzzy logic algorithm," *Mech. Sci.*, vol. 13, no. 2, pp. 713–724, 2022.

[30] Y. Wu, L. Wang, J. Zhang, and F. Li, "Path following control of autonomous ground vehicle based on nonsingular terminal sliding mode and active disturbance rejection control," *IEEE Trans. Veh. Technol.*, vol. 68, no. 7, pp. 6379–6390, Jul. 2019.

[31] J. M. Snider et al., "Automatic steering methods for autonomous automobile path tracking," Robotics Institute, Carnegie Mellon Univ., Pittsburgh, PA, Tech. Rep. CMU-RITR-09-08, 2009.

[32] Q. Ge, Q. Sun, S. E. Li, S. Zheng, W. Wu, and X. Chen, "Numerically stable dynamic bicycle model for discrete-time control," in *2021 IEEE Intell. Veh. Symp. Workshops*, 2021, pp. 128–134.

[33] P. Kachroo and M. Tomizuka, "Chattering reduction and error convergence in the sliding-mode control of a class of nonlinear systems," *IEEE Trans. Autom. Control*, vol. 41, no. 7, pp. 1063–1068, Jul. 1996.

[34] "Planning simulation. tutorial," Autoware Foundation, 2024. Accessed: 28, Feb. 2024 https://autowarefoundation.github.io/autoware-documentation/main/tutorials/ad-hoc-simulation/planning-simulation

[35] J. Matute, M. Rodriguez-Arozamena, J. Perez, and A. Karimoddini, "Sensor fusion-based localization framework for autonomous vehicles in rural forested environments," in *2023 IEEE 26th Int. Conf. Intell. Transp. Syst.*, 2023, pp. 1007–1013.

[36] T. Lee and Y. Jeong, "A tube-based model predictive control for path tracking of autonomous articulated vehicle," in *Actuators*, vol. 13, no. 5, 2024, Art. no. 164.